

# $K_3Fe(CN)_6$ : Pressure-Induced Polymerization and Enhanced Conductivity

Kuo Li,<sup>\*,†,‡,§,||</sup> Haiyan Zheng,<sup>†,‡</sup> Iliia N. Ivanov,<sup>⊥</sup> Malcolm Guthrie,<sup>†</sup> Yuming Xiao,<sup>#</sup> Wenge Yang,<sup>§,||</sup> Chris A. Tulk,<sup>∇</sup> Yusheng Zhao,<sup>○</sup> and Ho-kwang Mao<sup>†,‡,||</sup>

<sup>†</sup>Geophysical Laboratory, Carnegie Institution of Washington, Washington, DC 20015, United States

<sup>‡</sup>Center for High Pressure Science and Technology Advanced Research, P.O. Box 8009, Beijing 100088, China

<sup>⊥</sup>Center for Nanophase Materials Sciences and <sup>∇</sup>Spallation Neutron Source, Oak Ridge National Laboratory, Oak Ridge, Tennessee 37830, United States

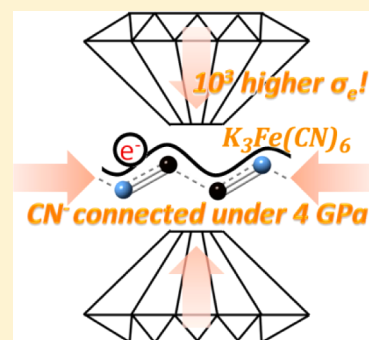
<sup>#</sup>HPCAT and <sup>§</sup>HPSynC, Geophysical Laboratory, Carnegie Institution of Washington, Argonne, Illinois 60439, United States

<sup>○</sup>HiPSEC and Department of Physics & Astronomy, University of Nevada, Las Vegas, Nevada 89154, United States

<sup>||</sup>Center for High Pressure Science and Technology Advanced Research, 1690 Cailun Rd., Pudong, Shanghai 201203, P.R. China

## Supporting Information

**ABSTRACT:** Recent theoretical studies indicate that applying high pressure (up to tens of gigapascals) to simple compounds with triple bonds can convert the triple bonds to conjugated double bonds, which results in these compounds becoming electrically conductive or even superconductive. This might indicate a new route for the synthesis of inorganic/organic conductors of various compositions and properties and could greatly expand the field of conductive polymers. Here, we present a study of the phase behavior and electrical properties of  $K_3Fe(CN)_6$  up to  $\sim 15$  GPa using Raman spectroscopy, synchrotron X-ray diffraction, and impedance spectroscopy at room temperature. In this pressure range, two new crystalline phases were identified, and their unit cells and space groups were determined. The cyanide ions react to form conjugated C=N bonds in two steps, and the electronic conductivity is enhanced by 3 orders of magnitude, from  $10^{-7}$  to  $10^{-4}$  S $\cdot$ cm $^{-1}$ . Because this material is also an ionic conductor, these studies might “shed light” on the development of new cathode materials for alkali metal batteries. Enhancing the electrical conductivity by applying high pressure to compounds containing triple bonds could provide a potential route for synthesizing multifunctional conductive materials.



## INTRODUCTION

Pressure-induced polymerization has recently become an interesting topic in chemistry, particularly with the development of modern ultrahigh-pressure devices. Applying pressure provides a route to overcome the barrier of repulsion between monomers, including both neutral and charged monomers. Furthermore, many traditional addition polymerization reactions can be induced by applying pressure,<sup>1–4</sup> and some unsaturated ionic monomers that do not polymerize at ambient pressure can be forced to polymerize under high pressure, for example,  $C\equiv N^-$  and probably  $C\equiv C^{2-}$ .<sup>5–9</sup> NaCN, a simple alkali metal cyanide, polymerizes irreversibly into an amorphous phase containing CN double bonds above 25 GPa.<sup>6</sup> The Prussian blue compound  $Fe[Co(CN)_6]$  amorphizes above 10 GPa, and the sample recovered at 17.4 GPa shows a feature in its Raman spectrum similar to that of an amorphous  $CN_x$  film.<sup>9</sup>  $BaC_2$  undergoes a similar irreversible phase transition above 30 GPa, as indicated by the disappearance of a  $C\equiv C$  stretching peak in its Raman spectrum.<sup>8</sup> Theoretical studies of the polymerization of acetylide, cyanide, and neutral molecules with cyano groups predicting many polymerized phases have been reported.<sup>10–13</sup> Some of the polymerized

phases have structures with conjugated double bonds and are expected to be conductors or superconductors, which has attracted more attention.<sup>10,12</sup> In general, atoms tend to bond to more neighbors under high pressure such that all kinds of the unsaturated groups can become connected.

$K_3Fe(CN)_6$  is an important and well-studied compound in coordination chemistry and electrochemistry.  $Fe(CN)_6^{3-}$  is a typical complex anion with strong field ligands and  $\pi$ -back bonding, and the  $Fe(CN)_6^{3-}/Fe(CN)_6^{4-}$  redox pair is often used as a reference in electrochemistry. In the 1960s and 1970s, several Mössbauer experiments indicated that Fe(III) in crystallized  $K_3Fe(CN)_6$  could be reduced to Fe(II) under high pressure, and subsequent research reported that the reduction was not caused by the application of hydrostatic pressure itself but rather by the shear deformation of the sample.<sup>14–17</sup> Transport measurements showed that the electrical resistance of  $K_3Fe(CN)_6$  has a minimum value at  $\sim 4$  GPa.<sup>16</sup> Recently, Raman spectroscopic studies have

Received: July 25, 2013

Revised: September 17, 2013

Published: October 18, 2013

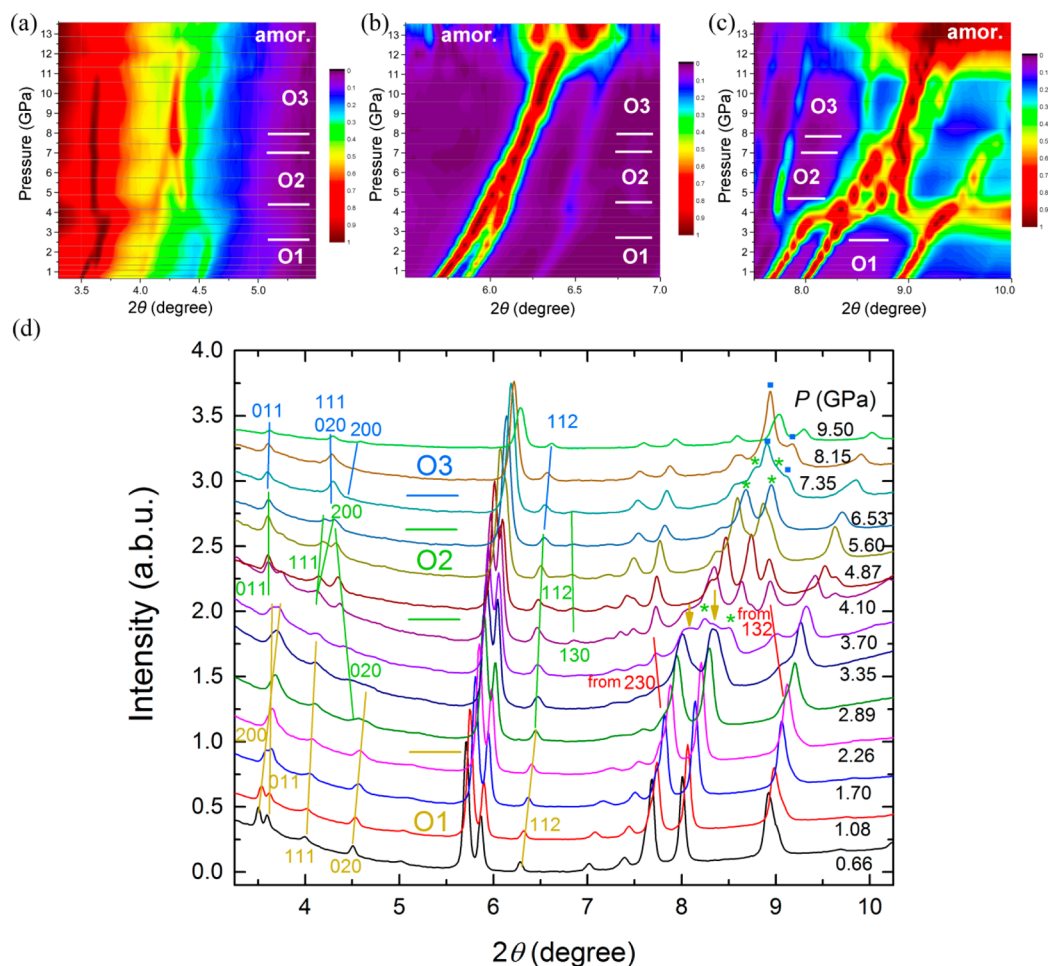


**Figure 1.** (a–c) Selected XRD patterns of  $\text{K}_3\text{Fe}(\text{CN})_6$  under high pressure. The intensities of each pattern are normalized to its maximum in the range of plot. Colors from red to violet represent intensities from high to low. The measured data are marked by gray lines, and the spaces between them are filled by the calculated color map. (d) Indices of selected isolated peaks. The yellow, green, and blue straight lines are guide for the eye. The peaks of O1–O3 are marked by yellow arrows, green stars, and blue squares, respectively, in the  $2\theta$  range of  $8\text{--}9^\circ$  and the pressure range of two-phase coexistence.

followed the change in the lattice mode frequencies with pressure and provided indirect indications of a phase transition at  $\sim 2.5$  GPa.<sup>18</sup> This research reveals the complicated interactions within  $\text{K}_3\text{Fe}(\text{CN})_6$  with applied pressure. In this work, we studied the changes in the structural and electrical properties of  $\text{K}_3\text{Fe}(\text{CN})_6$  up to  $\sim 15$  GPa using Raman spectroscopy, synchrotron angular-dispersive X-ray diffraction (ADXRD), and impedance spectroscopy. The evolution of the structure and electrical conductivity and their relation to one another are discussed. Additionally, a new route to prepare inorganic/organic multifunctional conductors is proposed.

## EXPERIMENTAL METHODS

For the in situ Raman and synchrotron ADXRD measurements, a fine powder of  $\text{K}_3\text{Fe}(\text{CN})_6$  (orthorhombic phase,<sup>19</sup> Sigma-Aldrich, particle size  $< 10$   $\mu\text{m}$ ) was gently ground in an agate mortar for less than 5 min before being loaded into a symmetric-style diamond anvil cell (DAC)<sup>20</sup> fitted with diamonds polished to a culet diameter of  $d_{\text{culet}} = 400$   $\mu\text{m}$ . T301 stainless steel gaskets were preindented to a thickness of  $\sim 30$   $\mu\text{m}$  and holes, with  $d = 200$   $\mu\text{m}$  were drilled in the center of the indentation to serve as the sample chamber. Neon was loaded as the pressure medium using the GSECARS' gas loading system<sup>21</sup> at sector 13 of the Advanced Photon Source

(APS), Argonne National Laboratory. Raman spectra were measured up to  $\sim 15$  GPa using a laboratory-made spectrometer equipped with a Nd:YAG laser (operating at 532 nm) in a backscattering geometry. The ADXRD data were collected up to  $\sim 15$  GPa at beamline 16-ID-D of APS. The monochromated incident X-ray wavelength was 0.40663 Å. The preliminary data reduction was performed using the Fit2D program.<sup>22</sup> In situ impedance spectroscopy was performed on an ac impedance spectroscopy system based on Zahner analyzer IM6 at the Center for Nanophase Materials Sciences, Oak Ridge National Laboratory. A symmetric DAC fitted with diamonds with  $d_{\text{culet}} = 500$   $\mu\text{m}$  was used in a four-probe (van der Pauw) setting, and ac voltage (50 mv) was applied in the frequency range between 0.1 Hz and 1 MHz. A steel-supported BN gasket and Pt foil electrodes were used for this measurement. The gasket was preindented to  $\sim 40$ - $\mu\text{m}$  thickness, and a hole with a diameter of  $\sim 200$   $\mu\text{m}$  was drilled in the indentation center. No pressure medium was used in the impedance measurements. Ruby fluorescence was used for pressure calibration in the experiments.<sup>23</sup>

## RESULT AND DISCUSSION

XRD data were collected with increasing pressure and show a clear progression of phase transitions; see Figure 1. At pressures

below 2.5 GPa,  $\text{K}_3\text{Fe}(\text{CN})_6$  retains its orthorhombic structure with the space group *Pnca* (hereafter referred to as phase O1).<sup>19</sup> At 2.9 GPa, a new reflection at  $2\theta \approx 4.5^\circ$  appears next to the 020 reflection (see Figure 1d). This peak moves to low angle with increasing pressure. Simultaneously, the intensity of the 020 reflection of the O1 phase is weakened, which is represented by the plotted color changing from green to blue in Figure 1a. The other two peaks, splitting from the 230 and 132 reflections of the O1 phase, at  $2\theta$  values of  $\sim 7.8^\circ$  and  $\sim 9.1^\circ$ , respectively, also move to lower angle with increasing pressure, shown as the branches of the main peaks (red) in Figure 1c and marked by red lines in Figure 1d. All of these changes indicate the onset of a phase transition. The new phase is hereafter referred to as O2. The superposition of diffraction spectra (indicating the coexistence of the two phases) becomes more obvious in the  $2\theta$  range of  $8.0\text{--}8.5^\circ$  at pressures above 3.70 GPa, as marked by yellow arrows and green stars, respectively (Figure 1d). Figure 1a–c illustrates a discontinuity in the pressure dependence of the peak position, which can be observed clearly between 2.5 and 4.0 GPa. This is a good indication that the phase transition starts at  $\sim 2.5$  GPa and is completed at  $\sim 4$  GPa; see the white bars in the figure. The data in Figure 1d illustrate the XRD reflections of phase O2 and those of another new phase in the  $2\theta$  range between  $8.5^\circ$  and  $9^\circ$  at 7.35 GPa, as indicated by the green stars and blue squares, respectively. This suggests yet another phase transition from phase O2 to a new phase (hereafter referred to as O3). Above  $\sim 12$  GPa, the intensities of the Bragg reflections decrease significantly, and severe peak broadening is observed, indicating the onset of amorphization (Figure S1, Supporting Information).

The reflections from both the O2 and O3 phases can be indexed with an orthorhombic unit cell by a trial-and-error method using the PowderX software.<sup>24</sup> The lattice parameters of phase O2 at 5.6 GPa are  $a = 10.9871(9)$  Å,  $b = 10.7470(9)$  Å, and  $c = 8.0964(5)$  Å, and those for phase O3 at 9.5 GPa are  $a = 10.083(2)$  Å,  $b = 10.851(2)$  Å, and  $c = 7.9914(6)$  Å. Although these values are similar to those of O1 phase, a refinement process starting with the unit cell of O1 does not converge to the unit cells determined using the PowderX software. With the clear exception of the new peak at  $2\theta = 6.86^\circ$ , all of the reflections from the O2 phase can be indexed using the *Pnca* space group of the O1 phase. However, removing the *a*-glide plane of the *Pnca* space group allows the new reflection to be indexed with 130 Miller indices (see Figure 1d). It should be noted that removal of the *a*-glide plane from the *Pnca* space group results in the *Pnc2* subgroup. Using the *Pnc2* space group allowed all reflections to be well fitted by the Pawley or LeBail method. (Note that the *Pnc2* space group also has the highest symmetry.) In phase O3, the weak reflections are difficult to differentiate, and as a result, the space groups *Pnc2* or *Pnca* cannot be distinguished; therefore, following the O2 phase, the *Pnc2* space group was selected. The pressure dependence of the fitted lattice parameters is shown in Figure 2, and as expected, discontinuities are found between phases. The unit cell of the O3 phase is selected with the *a* axis smaller than the *b* axis, so that the positions of the symmetry elements of the O2 phase are retained and the Miller indices of the reflections remain unchanged. Such a similarity of the lattice parameters and space groups between these three phases suggests that the phase transition might not be a complete structural reconstruction and that the atoms probably do not move too far after the phase transition.

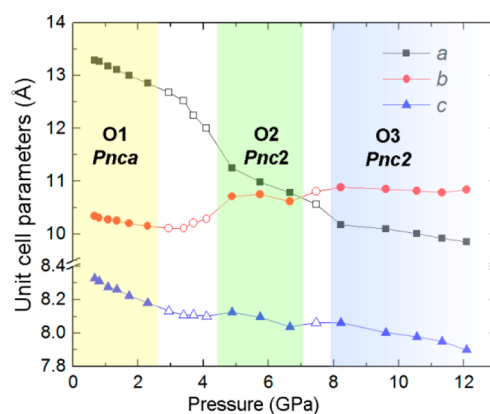


**Figure 2.** Lattice parameters of  $\text{K}_3\text{Fe}(\text{CN})_6$  under high pressure. The lattice parameters between O1 and O2 were refined with space group *Pnca* arbitrarily. Uncertainties provided by the fitting program are smaller than the label sizes.

In general, a phase transition from one space group to one of its subgroups can be caused by a lattice distortion and/or a rotation of polyhedra.<sup>25</sup> The Prussian blue compound is a typical example in the cyanide family. The  $\text{Fe}(\text{CN})_6^{3-}$  octahedron in  $\text{RbMn}[\text{Fe}(\text{CN})_6]$  rotates under applied pressure and results in the space group transforming from  $F\bar{4}3m$  to  $I\bar{4}m2$  at  $\sim 0.3$  GPa and subsequently to  $P\bar{4}n2$  at  $\sim 2.0$  GPa.<sup>26,27</sup> Another cyanide compound, NaCN, undergoes a sequence of space group transformations from  $Fm\bar{3}m$  to  $Immm$ ,  $Pmmm$ ,  $Cm$ , and  $P4mm$  with increasing pressure.<sup>6</sup> Most of these transitions are caused by the ordering of CN and/or distortion of the structure between a space group and its subgroup. In  $\text{K}_3\text{Fe}(\text{CN})_6$ , the  $\text{Fe}(\text{CN})_6^{3-}$  octahedron can distort and rotate as found in the Prussian blue compound under high pressure,<sup>9,27,28</sup> and relative displacement can happen between K and N as in NaCN. Because the CN–K bond is a nondirectional ionic bond, it can be thought of as somewhat “slippery”, whereas the Fe–CN bond is a coordinate bond, so that the Fe–C–N connection might twist, but it is not likely to break.

The compressibility of  $\text{K}_3\text{Fe}(\text{CN})_6$  is highly anisotropic, as shown in Figure 2. In all three phases studied here, the *a* axis always exhibits the highest compressibility, the *c* axis shows the lowest, and the *b* axis increases after the phase transition. This is probably related to the layered structure of the material. A structural model of  $\text{K}_3\text{Fe}(\text{CN})_6$  under ambient pressure<sup>19</sup> is shown in Figure 3. The regular octahedral geometry of the  $\text{Fe}(\text{CN})_6^{3-}$  group can be treated as a basic building block. Layers are formed by alternate packing of  $\text{Fe}(\text{CN})_6^{3-}$  units and K2 in a rectangular planar lattice. This structure can be viewed as a chain of edge-shared  $\text{Fe}(\text{CN})_6^{3-}$  and  $\text{KN}_6$  polyhedra along the *c* axis, with neighboring chains connected in the *b* direction by sharing the corners of the octahedra. K1 is located between the layers, bonding to two N atoms in one layer and four N atoms in the other layer. The packing inside the layer is more compact than that between the layers. Interlayer spaces can be found between K1, and the minimum distance between two N atoms from neighboring layers is  $\sim 3.8$  Å at ambient pressure, which is greater than the sum of the van der Waals radii ( $1.55 \text{ Å} \times 2 = 3.10 \text{ Å}$ ).<sup>29</sup> Such space is probably why the *a* axis is more compressible. Additionally, in the phase transition from O1 to O2, the *a* axis is significantly compressed, whereas the *b* axis is elongated. This could be caused by some bonds along the *a* axis before the transition rotating more along the *b* axis after the

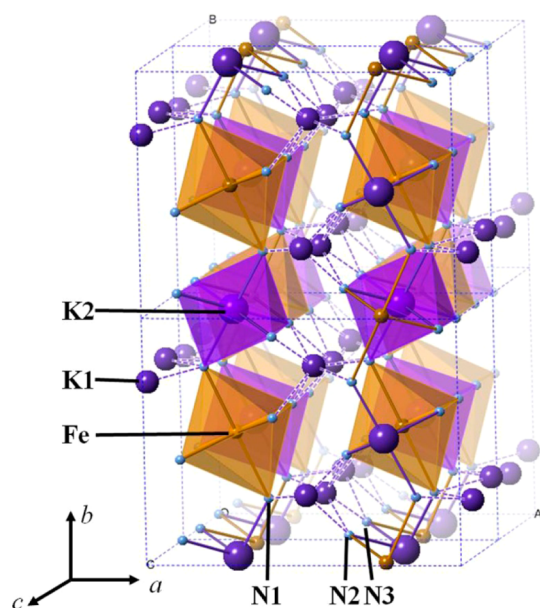


**Figure 3.** Structure model of the orthorhombic  $\text{K}_3\text{Fe}(\text{CN})_6$  phase (O1) at ambient pressure.  $\text{Fe}(\text{CN})_6^{3-}$  and  $\text{K}_2\text{N}_6$  are represented by brown and violet octahedra, respectively. The K1—N bond is represented by dashed lines between the layers. C atoms are not shown for clarity.

transition; as examples, the  $\text{C}\equiv\text{N}$  bonds and K—N bonds are noted. A similar report about Prussian blue compounds can be found in the literature.<sup>26,27</sup>

These phase transitions can also be observed in the Raman spectra. In the range of  $\Delta\nu < 500 \text{ cm}^{-1}$ , a new peak is observed at  $\Delta\nu \approx 300 \text{ cm}^{-1}$  when the sample is compressed to  $\sim 2.5 \text{ GPa}$ , as shown in Figure S2 (Supporting Information). Observation of the new peak at this pressure is consistent with a recent Raman study in which the starting material was believed to be the monoclinic phase<sup>19</sup> and the phase transition was attributed to the transition from monoclinic to orthorhombic phase.<sup>18</sup> In the current work, the XRD results identify the starting material as the orthorhombic phase, O1, and the phase transition at 2.5 GPa as being from the O1 phase to another orthorhombic phase, O2. The Raman data also show additional spectral changes at  $\sim 4$  and  $\sim 8 \text{ GPa}$ . The intensities of the  $\text{C}\equiv\text{N}$  stretching modes ( $\Delta\nu = 2129.7, 2132.3, \text{ and } 2139.0 \text{ cm}^{-1}$  at 1.21 GPa) decrease significantly by  $\sim 4 \text{ GPa}$ , indicating a likely reaction between some of the cyanide ions. The residual intensity disappears completely by  $\sim 8 \text{ GPa}$ , which indicates the completion of the reaction between the remaining cyanide ions (Figure 4a). These variations correspond to the phase transitions from O1 to O2 and from O2 to O3, respectively. The Raman spectra of phases O2 and O3 show new bands centered at  $\Delta\nu \approx 1450 \text{ cm}^{-1}$  and  $\Delta\nu \approx 1560 \text{ cm}^{-1}$  (Figure 4b). The latter can be recognized as the stretching mode of  $\text{C}=\text{N}$  or the G band similar to that found in the polymerized NaCN.<sup>6</sup> The wide band centered at  $\Delta\nu \approx 1450 \text{ cm}^{-1}$  correlates well with the D band that is induced by the disorder. Another weak band at  $\Delta\nu \approx 1020 \text{ cm}^{-1}$  likely corresponds to the stretching of a  $\text{C}-\text{N}$  or  $\text{C}-\text{C}$  bond; however, as pointed out in the literature, these two modes have similar Raman shifts, so the peak cannot be assigned definitively.<sup>30</sup> The disappearance of  $\text{C}\equiv\text{N}$  and the appearance of  $\text{C}=\text{N}$  and likely  $\text{C}-\text{N}$  (or  $\text{C}-\text{C}$ ) strongly suggest that the reaction serves to connect the cyanide ions,  $\text{CN}^-$ , together to form a polymer or at least

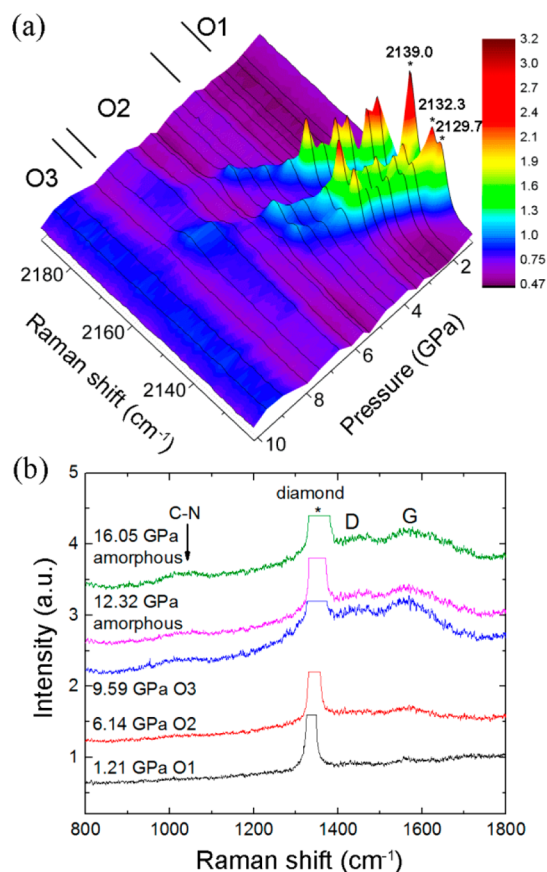


**Figure 4.** (a) Dynamic changes in the Raman spectrum of  $\text{CN}^-$  undergoing a high-pressure transition. The measured data are marked by solid lines, and the spaces between them are filled by the calculated color map. (b) Double bonds stretching in  $\text{K}_3\text{Fe}(\text{CN})_6$  under high pressure. All patterns were collected with the same laser power and collection time.

polymer fragments. To some degree, the structural transitions discussed above can be supported by this polymerization. The  $\text{CN}^-$  ions react with each other, which will certainly distort the  $\text{Fe}(\text{CN})_6^{3-}$  octahedron and, as such, drive the phase transition.

Similar results have also been found in the pressure-induced polymerization of NaCN and  $\text{FeCo}(\text{CN})_6$ .<sup>6,9</sup> The reaction of CN and the amorphization of NaCN [and  $\text{FeCo}(\text{CN})_6$ ] were observed at almost the same pressure, and thus, it was easy to conclude that the two are closely related and that either the polymerization of CN destroys the lattice and results in the amorphization of the materials or the amorphization activates the monomers and results in the polymerization. However, it is interesting that the phase transitions of  $\text{K}_3\text{Fe}(\text{CN})_6$  studied in this work indicate that the reaction between cyanide groups might not necessarily result in amorphization. This provides the future opportunity of characterizing the process of polymerization and studying the mechanism of the reaction between the neighboring CN groups with crystallographic methods.

Electronic and ionic conductivities can be distinguished from each other in the impedance spectrum. In a mixed electronic/ionic conductor, when blocking electrodes are used, the impedance is mostly attributed to electronic resistance ( $R_e$ ) at the low-frequency limit and the parallel connection of  $R_e$  and ionic resistance ( $R_i$ ) at the high-frequency limit.<sup>31,32</sup> A typical Nyquist plot of  $\text{K}_3\text{Fe}(\text{CN})_6$  at high pressure is shown in Figure S5a (with more examples given in Figure S3, Supporting

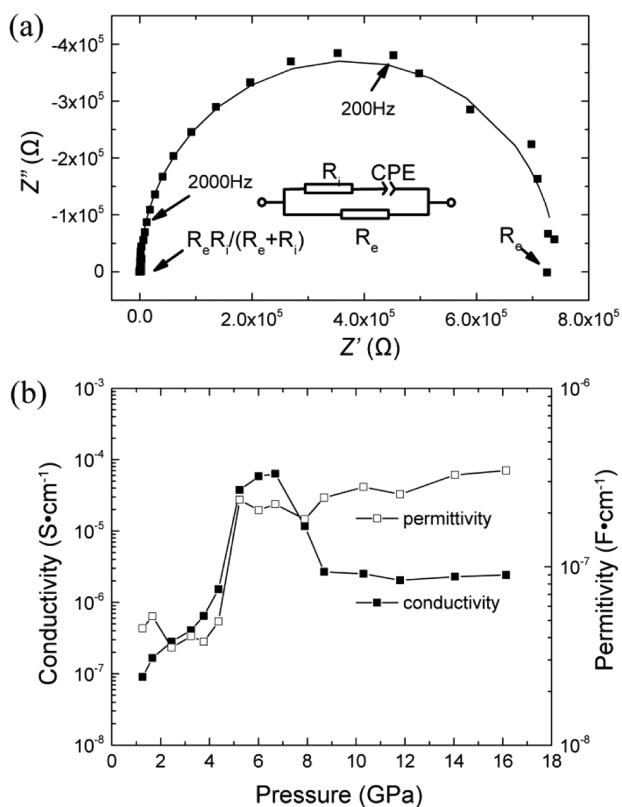


**Figure 5.** (a) Real and imaginary impedance of  $\text{K}_3\text{Fe}(\text{CN})_6$  (at  $\sim 6$  GPa) represented in a Nyquist plot. The solid line is the fitting curve, and the equivalent circuit is shown as well. (b) Electronic conductivity and permittivity of  $\text{K}_3\text{Fe}(\text{CN})_6$  under high pressure.

Information). In the plot,  $R_i R_e / (R_i + R_e) \approx 0$ , indicating that  $R_i$  is much smaller than  $R_e$ . Because the  $Z'$  axis uses a linear scale,  $R_i R_e / (R_i + R_e)$  cannot be measured accurately. In this work, we mainly focus on the electronic conductivity.

Within the van der Pauw configuration, the resistivity and permittivity of the corresponding arc in the Nyquist plot can be calculated (details are provided in the Supporting Information). At 4–5 GPa, the electronic conductivity exhibits a sharp increase and then remains almost constant until  $\sim 7$  GPa (Figure 5b). A plausible mechanism for the observed enhancement is the connection between cyanide ions, as shown by the Raman spectrum. Electrons can become more delocalized on the C, N, and probably Fe atoms, which enhances the electronic conductivity greatly, just as observed in conductive polymers. An additional possibility is electron transfer between connected CN groups and Fe, which actually dopes the connected CN groups and has been reported previously.<sup>14–16</sup> The decrease of the conductivity at 7–8 GPa can be attributed to the phase transition from phase O2 to phase O3. Samples synthesized at 9 and 20 GPa and recovered to ambient pressure are black, whereas those obtained at 4 and 6 GPa remain yellow. Such a change in optical absorption indicates a significant variation of the band structure and coordination of  $\text{Fe}^{3+}$ . Further explanation depends on the details of the crystal structure, which is the subject of ongoing research. In ref 16, a similar measurement of the resistance of  $\text{K}_3\text{Fe}(\text{CN})_6$  was reported. In that case, the resistance was measured directly in a two-electrode configuration. The result is qualitatively the same as that obtained in this work. The difference might be due to the starting materials, including the

type of crystalline phase, the grain size/grain boundary, and the apparatus used.

The apparent permittivity of  $\text{K}_3\text{Fe}(\text{CN})_6$  corresponding to the observed semicircle is  $\sim 10^{-7} \text{ F}\cdot\text{cm}^{-1}$  (Figure 5b). This is far greater than typical values for the bulk material ( $10^{-12} \text{ F}\cdot\text{cm}^{-1}$ ) or even ferroelectric phases ( $10^{-9} \text{ F}\cdot\text{cm}^{-1}$ ). It can be attributed only to double layer capacitance.<sup>33</sup> The capacitance per unit area of the electrode is approximately  $10^{-5} \text{ F}\cdot\text{cm}^{-2}$ , within the range of double layer capacitance.<sup>34</sup> The double layer capacitance was represented by a constant-phase element (CPE) in the equivalent circuit (Figure 5a, inset). This arises because the conducting ions are blocked by the metal electrodes (Pt) and charge only the double layer at the electrodes. It also shows an abrupt increase at  $\sim 4$ – $5$  GPa, corresponding to the phase transition from O1 to O2. A plausible mechanism is that more  $\text{K}^+$  ions contribute to the capacitance in phase O2 (and O3) than in phase O1.

The mixed conductivity of  $\text{K}_3\text{Fe}(\text{CN})_6$  and the application of the  $\text{Fe}(\text{CN})_6^{3-}/\text{Fe}(\text{CN})_6^{4-}$  redox pair in electrochemistry suggest that  $\text{K}_3\text{Fe}(\text{CN})_6$  processed under high pressure could potentially be used as a cathode material. Prussian blue compounds such as  $\text{KFe}_2(\text{CN})_6$  and  $\text{K}_{0.1}\text{Cu}[\text{Fe}(\text{CN})_6]_{0.7}\cdot 3.8\text{H}_2\text{O}$ , which have compositions and structures similar to those of  $\text{K}_3\text{Fe}(\text{CN})_6$ , have been studied as the cathode materials for alkali metal batteries.<sup>35,36</sup> Processing  $\text{K}_3\text{Fe}(\text{CN})_6$  with pressure to enhance its conductivity might also have such an application. Additionally, the connection of  $\text{CN}^-$  and the resulting enhancement in conductivity indicate that this process can potentially be used to synthesize C-based conductive materials with multifunctional properties. Other functional components, aside from triple bonds, could be contained in the starting materials, similarly to the way in which K and Fe are in this work, which could introduce exotic physical properties coupled with the electronic conductivity.

## CONCLUSIONS

This is the first systematic study of the crystal structure and electrical properties of  $\text{K}_3\text{Fe}(\text{CN})_6$  under high pressure. Two crystalline phases were found to be stabilized under high pressure and identified as O2 and O3, and their lattice parameters and space groups were determined by synchrotron XRD. O3 was observed to amorphize above 12 GPa. Evidence from Raman spectra show that the cyanide ions in  $\text{K}_3\text{Fe}(\text{CN})_6$  react with each other at pressures above 4 GPa and generate connected  $\text{C}=\text{N}$  bonds. The connection of cyanide groups enhances the electronic conductivity by  $\sim 3$  orders of magnitude, to  $\sim 10^{-4} \text{ S}\cdot\text{cm}^{-1}$ , which is higher than that of undoped polyacetylene.<sup>37</sup> Additionally, the pressure-induced polymerization of  $\text{K}_3\text{Fe}(\text{CN})_6$  involves a transition-metal element and results in good ionic conductivity. If the pressure of synthesis can be decreased, the resulting product could be a potential cathode material for alkali metal batteries, similarly to the Prussian blue materials.<sup>35,36</sup> In the view of synthetic chemistry, the story of  $\text{K}_3\text{Fe}(\text{CN})_6$  also suggests that the application of pressure can provide a new method for synthesizing conductors with multiple functionalities. For example, starting with a precursor with triple bonds and any other functional components, compression of the triple bonds to form conjugated double bonds can make the material conductive, thus combining this conductivity with the pre-existing properties.

## ■ ASSOCIATED CONTENT

### Supporting Information

Calculation of resistivity and permittivity with the four-probe van der Pauw setting, more examples of XRD and impedance spectra. This material is available free of charge via the Internet at <http://pubs.acs.org>.

## ■ AUTHOR INFORMATION

### Corresponding Author

\*E-mail: [kli@ciw.edu](mailto:kli@ciw.edu).

### Present Address

<sup>||</sup>SNAP, Spallation Neutron Source, Oak Ridge National Laboratory, Oak Ridge, TN 37830, United States.

### Author Contributions

The manuscript was written through contributions of all authors. All authors have given approval to the final version of the manuscript.

### Notes

The authors declare no competing financial interest.

## ■ ACKNOWLEDGMENTS

The authors appreciate Dr. X. Jing, Dr. E. A. Payzant, Dr. V. Struzhkin, and Dr. T. Muramatsu for their kind help. This work was supported as part of the Energy Frontier Research in Extreme Environment (EFREE) Center, an Energy Frontier Research Center funded by the U.S. Department of Energy (DOE), Office of Science, Basic Energy Sciences (BES), under Award DE-SC0001057. A portion of this research was performed at HPCAT (sector 16), Advanced Photon Source (APS), Argonne National Laboratory. HPCAT (Geophysical Laboratory) operations are supported by the DOE-NNSA under Award DE-NA0001974 and DOE-BES under Award DE-FG02-99ER45775, with partial instrumentation funding by the National Science Foundation (NSF). APS is supported by the DOE-BES, under Contract DE-AC02-06CH11357. A portion of this research was conducted at the Center for Nanophase Materials Sciences and Spallation Neutron Source, which are sponsored at Oak Ridge National Laboratory by the Scientific User Facilities Division, Office of Basic Energy Sciences, U.S. Department of Energy.

## ■ REFERENCES

- (1) Aoki, K.; Usuba, S.; Yoshida, M.; Kakudate, Y.; Tanaka, K.; Fujiwara, S. Raman Study of the Solid-State Polymerization of Acetylene at High Pressure. *J. Chem. Phys.* **1988**, *89*, 529–534.
- (2) Trout, C. C.; Badding, J. V. Solid State Polymerization of Acetylene at High Pressure and Low Temperature. *J. Phys. Chem. A* **2000**, *104*, 8142–8145.
- (3) Citroni, M.; Ceppatelli, M.; Bini, R.; Schettino, V. The High-Pressure Chemistry of Butadiene Crystal. *J. Chem. Phys.* **2003**, *118*, 1815–1820.
- (4) Santoro, M.; Ciabini, L.; Bini, R.; Schettino, V. High-Pressure Polymerization of Phenylacetylene and of the Benzene and Acetylene Moieties. *J. Raman Spectrosc.* **2003**, *34*, 557–566.
- (5) Heckathorn, J. W.; Kruger, M. B.; Gerlich, D.; Jeanloz, R. High-Pressure Behavior of the Alkali Cyanides KCN and NaCN. *Phys. Rev. B* **1999**, *60*, 979–983.
- (6) Chen, J. Y.; Yoo, C. S. Physical and Chemical Transformations of Sodium Cyanide at High Pressures. *J. Chem. Phys.* **2009**, *131*, 144507.
- (7) Dultz, W.; Krause, H. Light-Scattering Studies of the Polymorphism of Potassium Cyanide under Hydrostatic Pressure. *Phys. Rev. B* **1978**, *18*, 394–400.
- (8) Efthimiopoulos, I.; Kunc, K.; Vazhenin, G. V.; Stavrou, E.; Syassen, K.; Hanfland, M.; Liebig, St.; Ruschewitz, U. Structural

Transformation and Vibrational Properties of BaC<sub>2</sub> at High Pressure. *Phys. Rev. B* **2012**, *85*, 054105.

(9) Catafesta, J.; Haines, J.; Zorzi, J. E.; Pereira, A. S.; Perottoni, C. A. Pressure-Induced Amorphization and Decomposition of Fe[Co(CN)<sub>6</sub>]. *Phys. Rev. B* **2008**, *77*, 064104.

(10) Khazaei, M.; Tripathi, M. N.; Kawazoe, Y. First-Principles Simulation of Cyanogen under High Pressure: Formation of Paracyanogen and an Insulating Carbon Nitride Solid. *Phys. Rev. B* **2011**, *83*, 134111.

(11) Chen, X. Q.; Fu, C. L.; Franchini, C. Polymeric Forms of Carbon in Dense Lithium Carbide. *J. Phys.: Condens. Matter* **2010**, *22*, 292201.

(12) Li, Y. L.; Luo, W.; Zeng, Z.; Lin, H. Q.; Mao, H. K.; Ahuja, R. Pressure-Induced Superconductivity in CaC<sub>2</sub>. *Proc. Natl. Acad. Sci. U.S.A.* **2013**, *110*, 9289–9294.

(13) Chall, M.; Winkler, B.; Milman, V. Ab Initio Calculation of the High-Pressure Behaviour of Hydrogen Cyanide. *J. Phys.: Condens. Matter* **1996**, *8*, 9049–9057.

(14) Champion, A. R.; Drickamer, H. G. Effect of Pressure on the Mössbauer Resonance in Potassium Ferrocyanide, Potassium Ferricyanide, and Insoluble Prussian Blue. *J. Chem. Phys.* **1967**, *47*, 2591–2594.

(15) Fung, S. C.; Drickamer, H. G. Effect of Pressure on the C–Fe Bond in Ferrocyanides and Ferricyanides. *J. Chem. Phys.* **1969**, *51*, 4353–4359.

(16) Hara, Y.; Shirovani, I.; Minomura, S. Changes of the Electronic State and the Electrical Resistance of Some Iron Compounds at High Pressures. *Inorg. Chem.* **1975**, *14*, 1834–1837.

(17) Lewis, G. J.; Whalley, E. On the Supposed Pressure-Induced Reduction of Ferric Salts. *J. Chem. Phys.* **1980**, *72*, 2291–2294.

(18) Barsan, M. M.; Butler, I. S.; Fitzpatrick, J.; Gilson, D. F. R. High-Pressure Studies of the Micro-Raman Spectra of Iron Cyanide Complexes: Prussian Blue (Fe<sub>4</sub>[Fe(CN)<sub>6</sub>]<sub>3</sub>), Potassium Ferricyanide (K<sub>3</sub>[Fe(CN)<sub>6</sub>]), and Sodium Nitroprusside (Na<sub>2</sub>[Fe(CN)<sub>5</sub>(NO)]·2H<sub>2</sub>O). *J. Raman Spectrosc.* **2011**, *42*, 1820–1824.

(19) Figgis, B. N.; Skelton, B. W.; White, A. H. Crystal Structures of the Simple Monoclinic and Orthorhombic Polytypes of Tripotassium Hexacyanoferrate(III). *Aust. J. Chem.* **1978**, *31*, 1195–1199.

(20) Mao, H. K.; Bell, P. M. The Ultrahigh-Pressure Diamond Cell: Design Applications for Electrical Measurements of Mineral Samples at 1.2 Mbar. *Year Book—Carnegie Inst. Washington* **1976**, *75*, 824–827.

(21) Rivers, M.; Prakapenka, V. B.; Kubo, A.; Pullins, C.; Holl, C. M.; Jacobsen, S. D. The COMPRES/GSECARS Gas-Loading System for Diamond Anvil Cells at the Advanced Photon Source. *High Pressure Res.* **2008**, *28*, 273–292.

(22) Hammersley, A. P.; Svensson, S. O.; Hanfland, M.; Fitch, A. N.; Häusermann, D. Two-Dimensional Detector Software: From Real Detector to Idealised Image or Two-Theta Scan. *High Pressure Res.* **1996**, *14*, 235–248.

(23) Mao, H. K.; Xu, J.; Bell, P. M. Calibration of the Ruby Pressure Gauge to 800 kbar under Quasi-Hydrostatic Conditions. *J. Geophys. Res.-Sol. Ea.* **1986**, *91*, 4673–4676.

(24) Dong, C. PowderX: Windows-95-Based Program for Powder X-ray Diffraction Data Processing. *J. Appl. Crystallogr.* **1999**, *32*, 838–838.

(25) Glazer, A. M. The Classification of Tilted Octahedra in Perovskites. *Acta Crystallogr. B* **1972**, *28*, 3384–3392.

(26) Moritomo, Y.; Hanawa, M.; Ohishi, Y.; Kato, K.; Takata, M.; Kuriki, A.; Nishibori, E.; Sakata, M.; Ohkoshi, S.; Tokoro, H.; Hashimoto, K. Pressure- and Photoinduced Transformation into a Metastable Phase in RbMn[Fe(CN)<sub>6</sub>]. *Phys. Rev. B* **2003**, *68*, 144106.

(27) Liu, X. J.; Moritomo, Y.; Matsuda, T.; Kamioka, H.; Tokoro, H.; Ohkoshi, S. Pressure-Induced Octahedral Rotation in RbMn[Fe(CN)<sub>6</sub>]. *J. Phys. Soc. Jpn.* **2009**, *78*, 013602.

(28) Matsuda, T.; Liu, X. J.; Shibata, T.; Kamioka, H.; Ohishi, Y.; Moritomo, Y. Pressure-Induced Phase Transition in Zn–Fe Prussian Blue Lattice. *J. Phys. Soc. Jpn.* **2009**, *78*, 105002.

(29) Bondi, A. van der Waals Volumes and Radii. *J. Phys. Chem.* **1964**, *68*, 441–451.

(30) Ferrari, A. C.; Rodil, S. E.; Robertson, J. Interpretation of Infrared and Raman Spectra of Amorphous Carbon Nitrides. *Phys. Rev. B* **2003**, *67*, 155306.

(31) Wang, C.; Hong, J. Ionic/Electronic Conducting Characteristics of  $\text{LiFePO}_4$  Cathode Materials. The Determining Factors for High Rate Performance. *Electrochem. Solid-State Lett.* **2007**, *10*, A65–A69.

(32) Jamnik, J. Impedance Spectroscopy of Mixed Conductors with Semi-Blocking Boundaries. *Solid State Ionics* **2003**, *157*, 19–28.

(33) Irvine, J. T. S.; Sinclair, D. C.; West, A. R. Electroceramics: Characterization by Impedance Spectroscopy. *Adv. Mater.* **1990**, *2*, 132–138.

(34) Boukamp, B. A. Electrochemical Impedance Spectroscopy. Presented at *Nano-Electrochemistry*, Leiden, The Netherlands, Nov 24–28, 2008.

(35) Asakura, D.; Li, C. H.; Mizuno, Y.; Okubo, M.; Zhou, H.; Talham, D. R. Bimetallic Cyanide-Bridged Coordination Polymers as Lithium Ion Cathode Materials: Core@Shell Nanoparticles with Enhanced Cyclability. *J. Am. Chem. Soc.* **2013**, *135*, 2793–2799.

(36) Lu, Y.; Wang, L.; Cheng, J.; Goodenough, J. B. Prussian Blue: A New Framework of Electrode Materials for Sodium Batteries. *Chem. Commun.* **2012**, *48*, 6544–6546.

(37) Chiang, C. K.; Fincher, C. R.; Park, Y. W.; Heeger, A. J.; Shirakawa, H.; Louis, E. J.; Gau, S. C.; MacDiarmid, A. G. Electrical Conductivity in Doped Polyacetylene. *Phys. Rev. Lett.* **1977**, *39*, 1098–1101.